Research Article

Jeffrey Simon, Kyu Ri Choi, Stefano Ippolito, Ludmila Prokopeva, Colton Fruhling, Vladimir M. Shalaev, Alexander V. Kildishev, Yury Gogotsi and Alexandra Boltasseva*

Tailoring optical response of MXene thin films

https://doi.org/10.1515/nanoph-2024-0769
Received December 24, 2024; accepted March 19, 2025; published online April 3, 2025

Abstract: Due to their attractive optical properties, 2D MXenes have garnered interest in nanophotonic and optoelectronic applications. However, tuning their properties typically requires the iterative synthesis of MXenes with a specific set of properties, such as the absorption band position, electronic conductivity, and dielectric constant. We demonstrate how to tailor the optical properties of MXene thin films over a broad 1500-nm wavelength range by mixing different ratios of highly conductive $Ti_3C_2T_x$ with poorly conductive Nb_2CT_x. By changing the MXene film composition, the epsilon-near-zero (ENZ) point, where the optical properties transit from dielectric to metallic, was varied in the spectral range from 1.1 to 2.6 μm. Additionally, we observed a reduction in absorption in some compositions compared to the absorption of the pure MXene films. Compared to other methods, this approach enables simple and continual tuning of MXene optical properties without requiring multiple time-consuming synthesis steps.

Keywords: MXenes; 2D materials; plasmonics; solution processing; optical tunability; ENZ properties

Jeffrey Simon and Kyu Ri Choi contributed equally to this work.

***Corresponding author: Alexandra Boltasseva**, Elmore Family School of Electrical and Computer Engineering, Birck Nanotechnology Center and Purdue Quantum Science and Engineering Institute, Purdue University, West Lafayette, IN, 47907, USA; and School of Materials Engineering, Purdue University, West Lafayette, IN, 47907, USA,
E-mail: aeb@purdue.edu. https://orcid.org/0000-0001-8905-2605
Jeffrey Simon, **Ludmila Prokopeva**, **Colton Fruhling**, **Vladimir M. Shalaev and Alexander V. Kildishev**, Elmore Family School of Electrical and Computer Engineering, Birck Nanotechnology Center and Purdue Quantum Science and Engineering Institute, Purdue University, West Lafayette, IN, 47907, USA. https://orcid.org/0000-0002-8983-7055 (J. Simon).
https://orcid.org/0000-0003-4967-7461 (L. Prokopeva)
Kyu Ri Choi, Elmore Family School of Electrical and Computer Engineering, Birck Nanotechnology Center and Purdue Quantum Science and Engineering Institute, Purdue University, West Lafayette, IN, 47907, USA; and Research Institute for Nanoscale Science & Technology, Chungbuk National University, Cheongju, Chungbuk, 28644, Republic of Korea
Stefano Ippolito and Yury Gogotsi, A. J. Drexel Nanomaterials Institute and Department of Materials Science and Engineering, Drexel University, Philadelphia, PA, 19104, USA, E-mail: si368@drexel.edu (S. Ippolito). https://orcid.org/0000-0002-6906-3961 (S. Ippolito)

1 Introduction

MXenes, two-dimensional transition-metal carbides, nitrides, and carbonitrides, have the general formula $M_{n+1}X_nT_x$, where M represents an early transition metal, X is carbon and/or nitrogen, n ranges from 1 to 4, and T_x represents the surface terminations. The surface terminations are commonly a mixture of −O, −F, and −OH groups when the standard wet-chemical etching process is used [1], [2]. The family of MXenes includes dozens of currently synthesized single- and multi-transition metal compositions and supports a wide variety of optical properties, including dielectric, metallic, and theoretically predicted topological insulator behaviors [3]–[5], leading to a broad range of applications. For instance, MXenes have been utilized as substrates for surface-enhanced Raman scattering (SERS) [6], saturable absorber elements in mode-locked lasers [7]–[10], absorber materials in photodetectors [11], [12], and a broadband metamaterial absorber [13].

MXene films consist of a stacked layer-like arrangement of flakes (Figure 1a). They are usually deposited onto substrates using various solution-based processes, including spin, dip, or spray coating [14]. The resulting film's optical properties depend on the flake's electronic band structure, average size, and overall architecture (i.e., the physical arrangement of flakes within the film) [15]. Importantly, the straightforward deposition methods enable the formation of thin and homogeneous films of both optically dielectric and metallic MXenes without high-temperature steps, making MXenes promising and easy-to-process materials for applications in optical devices.

The success of any material for device design relies on the tunability of its optical properties, which is an active area of research for MXenes. This includes the synthesis of MXenes with different transition metals to discretely tune their optical properties [16]. Furthermore, continuous tunability can be achieved through solid-solution MXenes by

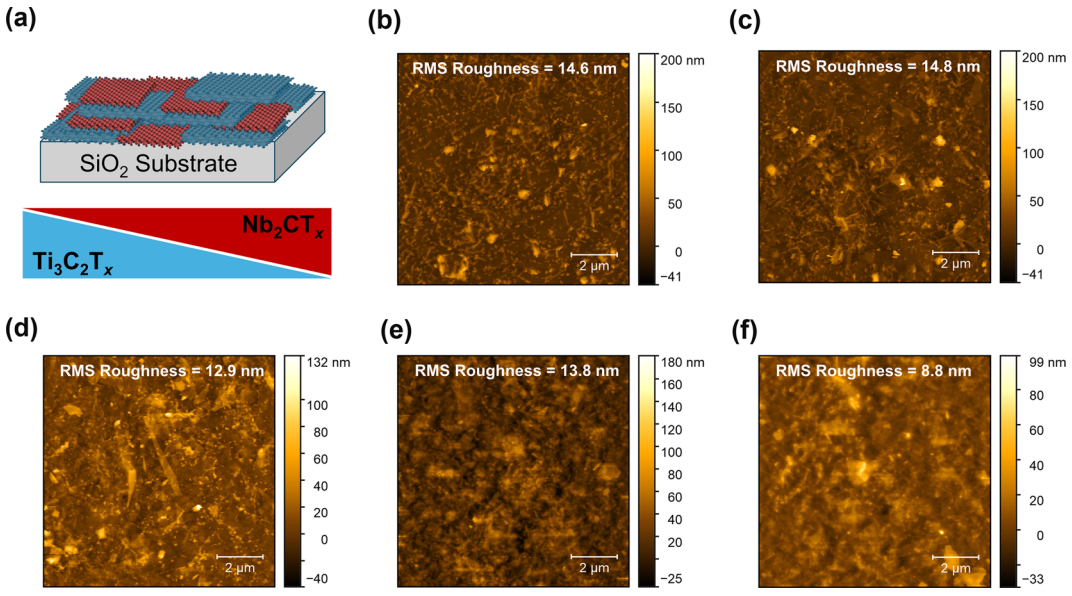

Figure 1: Randomly stacked MXene films. (a) A schematic representation of (top) a mixed film of $Ti_3C_2T_x$ and Nb_2CT_x MXene flakes with (bottom) concentrations that can be continuously varied. AFM images of (b) $Ti_3C_2T_x$, (c) $Ti_3C_2T_x$(75):Nb_2CT_x(25), (d) $Ti_3C_2T_x$(50):Nb_2CT_x(50), (e) $Ti_3C_2T_x$(25):Nb_2CT_x(75), and (f) Nb_2CT_x mixed-MXene films.

preparing the MAX phase with a desired ratio of two transition metal elements. Nevertheless, the optimization process is complex, requiring the synthesis of new MAX phases for each iteration [17]. While the flake size and film thickness are also shown to affect the optical properties [13], [15], the realization of large-scale and tailorable MXene films has not been reported. Other techniques for optical control that rely on the selection of surface terminations through annealing, molten-salt etching, and dynamic techniques are effective but have limited tunability range, issues with environmental stability, and affect the flake morphology [18]–[22].

This work introduces a simple approach to continuously tailor the optical properties through mixed-MXene films by precisely controlling their composition ratios (Figure 1a). $Ti_3C_2T_x$ has an epsilon-near-zero (ENZ) point in the near-infrared (NIR), where the optical properties transition from dielectric to metallic and the real part of the dielectric permittivity, $\Re(\varepsilon)$, crosses zero. The ENZ point is particularly interesting for optical applications since it has been shown to support unique propagating modes and enhance optical nonlinearities through the slow-light effect [23], [24]. In contrast to $Ti_3C_2T_x$, Nb_2CT_x acts as a dielectric across a broad optical spectrum. By combining these two MXenes, the film's optical properties could be tuned across the visible and short-wave infrared (SWIR) spectra. In addition to variable angle spectroscopic ellipsometry (VASE), the optical responses of the fabricated mixed-MXene films were characterized by UV-visible (VIS)-infrared (IR) reflection, transmission, and absorption spectroscopy. We found that as the concentration of Nb_2CT_x increased, the mixed-MXene films still exhibited metallic properties while their losses decreased. By changing the film composition, we observed the dramatic tuning of both the ENZ point and the plasma frequency, with respective redshifts of 1,500 nm and 2 eV.

2 Results

Five mixed-MXene thin films were fabricated by spray coating dispersions having different mass ratios of $Ti_3C_2T_x$ and Nb_2CT_x onto fused silica substrates (See Methods). This formed randomly stacked films (Figure 1a), with an average thickness of 30 nm (see S1) and varied morphology with respect to the composition of the constituent MXenes (Figure 1b–f). The majority of $Ti_3C_2T_x$ flakes were single layers with a lateral size typically ranging from 5-10 µm [25], while Nb_2CT_x flakes had lateral dimensions 5–10 times smaller and a higher percentage of few-layer nanosheets [26]. While each film had a similar RMS surface roughness on the scale of 10 nm, the films with higher $Ti_3C_2T_x$ ratios exhibited more fine wire-like features, representing wrinkles and ripples. Since both the spatial scale of the film roughness and flake thickness were deeply subwavelength, effective media behavior is expected [27].

A comprehensive study to investigate the linear optical properties of mixed-MXene films was performed, focusing on transmission enhancement and absorption reduction as the film composition changed. For films with higher

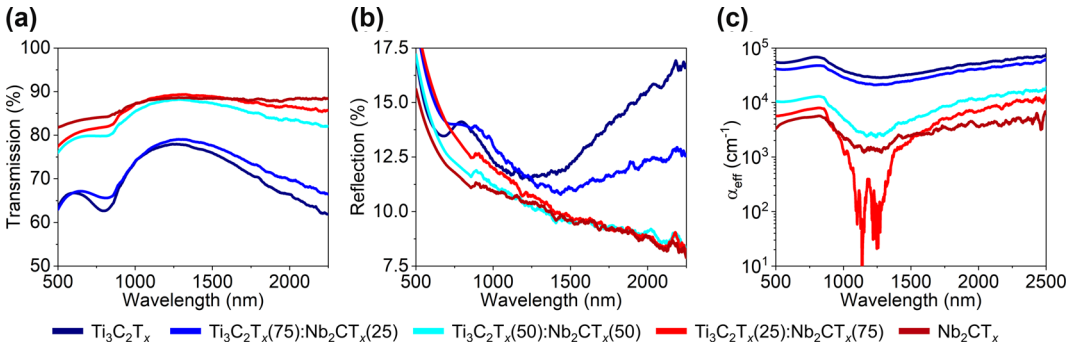

Figure 2: UV-VIS-IR spectroscopy measurements. (a) Transmission and (b) reflection spectra of $Ti_3C_2T_x$: Nb_2CT_x mixed-MXene. (c) Absorption coefficients of $Ti_3C_2T_x$: Nb_2CT_x mixed-MXene films.

$Ti_3C_2T_x$ concentrations, both the transmission and absorption spectra exhibited an increase in resonance strength near 800 nm (Figure 2a–c). Additionally, mixed films with higher Nb_2CT_x concentrations exhibited a pronounced improvement in optical transmission and a two-order-of-magnitude decrease in absorption across certain regions of the measured spectral range. This trend indicates that the inclusion of Nb_2CT_x contributed to the reduction in optical losses, potentially through the changes in the electronic and structural properties of the mixed films. An anomalous yet intriguing result was the remarkably low absorption observed in the film of $Ti_3C_2T_x$(25):Nb_2CT_x(75) between 750 and 1,500 nm, exhibiting losses lower than that of the pure films of $Ti_3C_2T_x$ or Nb_2CT_x (Figure 2c).

Additionally, films with higher $Ti_3C_2T_x$ concentrations exhibit a steeper slope in the reflection spectrum between 1,300 and 1,700 nm (Figure 2b). This behavior is likely due to the metallic properties of $Ti_3C_2T_x$, which strongly influence the optical response in the infrared region. The interplay of transmission enhancement, reduced absorption, and increased reflection highlights the complex optical nature of mixed-MXene films. It also underscores the importance of further exploring compositional control in tailoring the films' optical performance through VASE.

The Drude-Lorentz model was used to fit the VASE data and retrieve the real, $\Re(\varepsilon)$, and imaginary, $\Im(\varepsilon)$, components of the dielectric permittivity of the mixed-MXene thin films (Figure 3a–d). Both $\Re(\varepsilon)$ and $\Im(\varepsilon)$ fall between the pure titanium- and niobium-based films. The metallic optical properties indicated by the IR tail (Figure 3a) were parameterized in terms of the plasma frequency and ENZ wavelength (Figure 3d). Notably, the ENZ wavelength was in the SWIR spectrum and exhibited a substantial redshift of 1,500 nm as the $Ti_3C_2T_x$ concentration decreased. The redshift was induced by the change in the plasma frequency of the films, which varied from 1.25 eV to 3.09 eV as a function of composition (Figure 3d). This result highlights the continuous tunability of the metallic properties of the films controlled by the mass composition. In contrast to the $Ti_3C_2T_x$-based conducting films exhibiting Drude dispersion, pure Nb_2CT_x-based films are optically dielectric, with their NIR dispersion fitted by a heavily damped Lorentz, preventing the ENZ from occurring. The resonant frequencies of the Lorentzian fits, ω_{L1}, ω_{L2}, and ω_{L3}, were similar across all samples (Figure 3c). The ω_{L1} resonance at approximately 5.4 eV appeared in niobium-containing films, while the ω_{L3} resonance at 1.6 eV and the ω_{L2} resonances ranging from 3.5–4.5 eV were seen in the titanium-containing films. The complete Drude–Lorentz oscillator parameters are provided in the Supplementary Material.

3 Discussion

The mixed-MXene films contained two different types of resonances represented by the Drude-Lorentz model. The Drude portion represents the effects of free-carrier plasma oscillations, while the Lorentz terms could signify interband or other optical transitions. Focusing first on the Lorentz terms, we note that the transition energies were maintained across films with different MXene ratios (Figure 3c). This consistency suggests that the influence of neighboring MXenes on the band structure was minimal, unlike in other 2D material systems such as graphene [28]. On the contrary, the Drude term represented by the plasma frequency was influenced by the MXene composition. The plasma frequency exhibited a blue shift as $Ti_3C_2T_x$ increased, which we attribute to increasing carrier density according to the equation $\omega_p = \sqrt{N_c q^2/\varepsilon_0 m^*}$, where N_c is the free carrier density, q is the charge of an electron, ε_0 is the dielectric permittivity of free space, and m^* is the electron's effective mass [27]. From this equation and the non-square-root dependence of the plasma frequency on the concentration, we can deduce that the electrons provided by the $Ti_3C_2T_x$ are influenced by more complex interactions, such

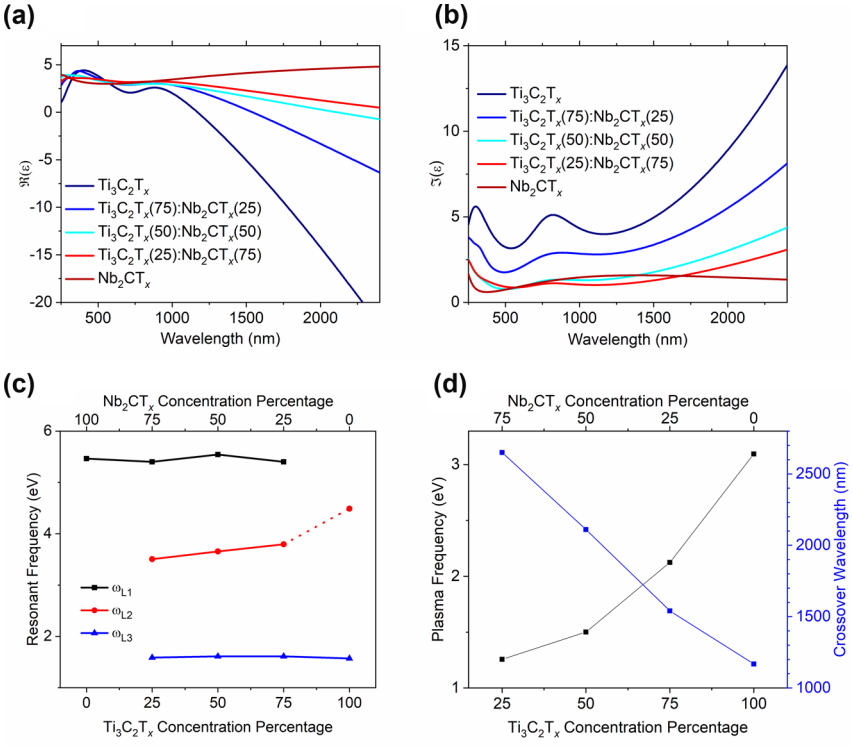

Figure 3: Dielectric permittivity values (a) real and (b) imaginary of $Ti_3C_2T_x$ and Nb_2CT_x mixed-MXene films. (c) Lorentz resonance frequencies plotted versus $Ti_3C_2T_x$ concentration percentage. (d) Plasma frequency and the dielectric permittivity $\Re(\varepsilon)$ zero-crossing point plotted versus $Ti_3C_2T_x$ concentration percentage. Note that the ω_{L2} resonance is associated with a higher frequency Lorentz oscillator for the pure $Ti_3C_2T_x$ film for consistency.

as charge transfer mechanisms between flakes or alternative interactions.

Notably, in the spectral region of approximately 900–1,400 nm, $\Im(\varepsilon)$of the mixed films of $Ti_3C_2T_x$(50):Nb_2CT_x(50) and $Ti_3C_2T_x$(25):Nb_2CT_x(75) had lower losses compared to the pure Nb_2CT_x film (Figure 3b), and is observation was corroborated by the UV-VIS-IR absorption data (Figure 2c). The underlying reasons for this unexpectedly low loss in mixed-MXene films remain to be fully elucidated. Interestingly, we note that for the $Ti_3C_2T_x$(25):Nb_2CT_x(75) film, the plasma frequency ω_p, a Lorentz resonance ω_{L3}, and the spectral window of decreased absorption all coincide, suggesting a synergistic interaction between the optically metallic $Ti_3C_2T_x$ and dielectric Nb_2CT_x. Other considerations should include the packing density of the mixed films, the difference in flake size, and morphology [29]–[31]. Compared to Nb_2CT_x flakes, the $Ti_3C_2T_x$ flakes were more monolayered, and 5–10 times larger, which potentially improved the packing density and resulted in reduced loss due to scattering. Interestingly, as the concentration of $Ti_3C_2T_x$ decreased in the film, the fine wire-like features also diminished (Figure 1b–f).

Interpreting the physical mechanisms behind tuning and reduced absorption requires further exploration into the complex electronic and optical environments of MXene flakes and films. In optical characterization, effects arising from mixed-termination MXenes, flake interactions, and polarizability dynamics due to disordered flake arrangements manifest as inhomogeneous broadening. Analyzing oscillator lineshapes presented in ellipsometry measurements could provide further insights. For example, modeling the absorption peaks with flexible lineshapes [32] revealed a stark difference in the nature of the Lorentzian peaks. The pure $Ti_3C_2T_x$ films, where the ω_{L3} peak was purely Lorentzian, and ω_{L2} the peak had significant inhomogeneous broadening (see Supplementary Material). Although beyond the paper's scope, the effects could be further resolved through monitoring carrier coherence dynamics with complex Fourier transform spectroscopy measurements [33].

The tunability and reduced loss of mixed-MXene films could support interesting optical applications. One exciting avenue of such characteristics is the control of the ENZ optical properties [25]–[31]. In pure $Ti_3C_2T_x$, optical losses must be reduced for the strong manifestation of ENZ phenomena. We uniquely demonstrated that mixing an optically metallic and dielectric MXene reduced optical losses and simultaneously tuned the ENZ wavelength. In contrast, tuning the

ENZ spectral range of organic materials by combining two distinct components often diminishes ENZ effects due to the disruptions in molecular aggregation [34]. Additionally, MXenes are known to have strong saturable absorption nonlinear optical properties in the infrared spectrum overlapping with important telecom and fiber laser operation wavelengths. A nonlinear enhancement due to the ENZ effects in mixed-MXene films could further enhance relevant technological applications.

Mixed-MXene films provide two knobs of tunability, where the first selects the Lorentz frequency through the choice of MXene, and the second controls plasma frequency – the Drude term – via the relative concentration of the two MXenes. Having two knobs for tunability in the mixed films enables easy optimization of resonance wavelengths. In contrast, tailoring solid solution MXenes through composition affects the position of the Lorentz resonances [17].

Future work includes optimizing the optical properties of mixed-MXene films iteratively by combining multiple MXenes and developing predictive models similar to Shrestha et al. [35]. Such models could incorporate compositional tuning, structural characteristics, and interfacial charge dynamics to physically understand and further enhance the performance of this novel composite material. By integrating experimental observations with advanced theoretical frameworks, the potential of mixed-MXene films as next-generation optical materials can be fully realized. This experimental study guides future research to explore additional material combinations, refine optical models, and advance the design of low-loss, tunable, and highly functional thin-film systems.

4 Conclusions

In conclusion, this study experimentally demonstrated a simple yet highly effective method to tailor the optical properties of MXene films by mixing MXenes with distinct compositions and features. We observed substantial tunability of the real part of the dielectric permittivity ENZ point ranging from 1.1 μm for a pure $Ti_3C_2T_x$ film to 2.6 μm for the $Ti_3C_2T_x$(25):Nb_2CT_x(75) film. The obtained ENZ point tunability exceeded previously reported ranges by over an order of magnitude, opening new possibilities for MXene applications by leveraging enhanced optical nonlinearities, such as the slow-light effect [23], [24], [36].

By systematically varying the relative concentrations of optically metallic $Ti_3C_2T_x$ and dielectric Nb_2CT_x, we observed distinct and highly tunable optical behaviors. Notably, the optical losses within the films were significantly reduced with increased Nb_2CT_x concentration, marking a substantial improvement in optical performance. This loss reduction was particularly noteworthy as high intrinsic losses in $Ti_3C_2T_x$ have been a limiting factor for optical and plasmonic applications. Incorporating Nb_2CT_x effectively mitigated this drawback, both preserving and potentially enhancing ENZ effects.

This proof-of-principle demonstration of mixed-MXene films represents a significant advancement, building upon the diverse optical properties offered by the extensive family of MXenes, including those in the IR range [36]. The straightforward methodology presented here opens new pathways for designing optical materials with unprecedented versatility and customization. The fabrication of mixed-MXene films uniquely leverages the simplicity of solution-based techniques to rapidly prepare and iterate samples with broad optical tunability. This capability contrasts with the synthesis-intensive approach required for solid-solution films, where each stoichiometry demands a distinct material preparation [17]. Our approach makes it possible to effectively "edit" the material's optical properties for applications that exploit light–matter interactions, such as advanced optical modulators, sensors, and nonlinear optical devices. The simplicity of tailoring the dielectric permittivity, combined with the reduction in optical losses, makes these systems highly versatile for applications requiring precise control over optical properties.

5 Materials and methods

5.1 MXene synthesis

One gram of stoichiometric Ti_3AlC_2 MAX powder (produced following our previously reported synthesis protocols) [37] was slowly added to a 20 mL mixture of concentrated HF (49 wt%), concentrated HCl (36 wt%), and deionized water, with a volumetric ratio of 1:6:3. The MAX phase was etched at 35 °C for 24 h. After the reaction was completed, the etching product was washed with deionized water via multiple centrifugation steps (3,500 rpm, 5 min) until neutral pH. To delaminate the MXene sheets, the $Ti_3C_2T_x$ multilayer product was stirred at 300 rpm in a 50 mL aqueous solution containing 1 g of LiCl at 35 °C for 18 h. Then, LiCl was removed from the solution by a single centrifugation step (3,500 rpm, 5 min), discarding the clear supernatant. After that, $Ti_3C_2T_x$ was redispersed in water via shaking and centrifuged for 15 min at 3,500 rpm (to precipitate the multilayer MXene and unreacted MAX particles). Finally, the dark supernatant (containing single-layer MXene sheets) is collected.

One gram of Nb_2AlC MAX powder was etched in a 20 mL mixture of HCl and HF, with a volume ratio of 12:8 at 48 °C for 50 h. After etching, the solution was repeatedly centrifuged with DI water at 3,500 rpm for 2 min until pH > 6. The obtained sediment was collected for delamination. The MXene flakes were delaminated using tetramethylammonium hydroxide (TMAOH). In particular, 5 mL of 25 wt% TMAOH solution was added to 1 g of etched MXene and stirred for 12 h at 35 °C. After that, the mixture was repeatedly centrifuged with DI water at 3,500 rpm for 10 min until pH < 8. Following delamination, the MXene dispersion was concentrated via high-speed centrifugation at 10,000 rpm.

5.2 Spray coating of film

Before use, the fused silica substrates were cleaned in a sonication bath in acetone and 2-propanol for 10 min each. After that, they were heated on a hot plate at 60 °C. Then, $Ti_3C_2T_x$, Nb_2CT_x, and their mixtures (aqueous dispersions with a concentration of ≈0.5 mg/mL) were sprayed using a commercial airbrush gun with a needle and nozzle diameter equal to 0.3 mm. The distance between the nozzle tip and the substrate was kept at about 20 cm. We describe the mixed films by $Ti_3C_2T_x$(Y):Nb_2CT_x(100-Y), where Y is the mass percentage of $Ti_3C_2T_x$ in the film.

5.3 Optical characterization

One mixed-MXene film was characterized for each concentration. We employed two standard techniques to characterize the optical properties of the fabricated thin films. Transmission and reflection spectra were measured with a Perkin Elmer Lambda 950 UV-VIS-NIR spectrometer. The subsequently calculated absorption was then used to identify optical transitions. The complex refractive index and permittivity were retrieved via spectroscopic ellipsometry (J. A. Woollam R2C VASE). Data was collected over a broad spectral (210–2,500 nm) and angular (55–75°) range to ensure unique fitting. The data was fitted alongside the transmission spectrum, and optical parameters were extracted with the CompleteEASE software.

Acknowledgements: We would like to thank Tetiana Parker at Drexel University for synthesizing the Nb_2CT_x MXene.

Research funding: This work was supported in part by the U.S. Department of Energy, Office of Basic Energy Sciences, Division of Materials Sciences and Engineering under Award DE-SC0017717 and the National Science Foundation (NSF) under the DMREF award 10002504. JS acknowledges support from the National Science Foundation Graduate Research Fellowship, award DGE-1842166. KC acknowledges support by the National Research Foundation of Korea (RS-2024-00352109). SI and YG acknowledge the Army Research Laboratory for supporting this work under Cooperative Agreement no. W911NF-19-2-0119. Any opinions, findings, conclusions, or recommendations expressed in this material are those of the authors(s) and do not necessarily reflect the views of the National Science Foundation.

Author contributions: All authors have accepted responsibility for the entire content of this manuscript and consented to its submission to the journal, reviewed all the results and approved the final version of the manuscript. JS and KC contributed equally to this work. JS contributed to the experiment's conception, optical measurements, and writing of the paper. KC contributed to optical measurements, data analysis, and the writing of the paper. SI contributed to the experiment's conception, MXene synthesis, and film deposition. CF contributed to the experiment's conception and the writing of the paper. LP contributed to data analysis. VMS, AVK, YG, and AB supervised various parts of the project and contributed to manuscript review and organization.

Conflict of interest: Authors state no conflict of interest.

Data availability: The datasets generated and/or analyzed during the current study are available from the corresponding author upon reasonable request.

References

[1] A. VahidMohammadi, J. Rosen, and Y. Gogotsi, "The world of two-dimensional carbides and nitrides (MXenes)," *Science*, vol. 372, no. 6547, p. eabf1581, 2021.

[2] K. R. G. Lim, M. Shekhirev, B. C. Wyatt, B. Anasori, Y. Gogotsi, and Z. W. Seh, "Fundamentals of MXene synthesis," *Nat. Synth.*, vol. 1, no. 8, p. 601, 2022.

[3] J. Simon, C. Fruhling, H. Kim, Y. Gogotsi, and A. Boltasseva, "MXenes for optics and photonics," *Opt. Photonics News*, vol. 34, no. 11, p. 42, 2023.

[4] X. Jiang, *et al*., "Two-dimensional MXenes: from morphological to optical, electric, and magnetic properties and applications," *Phys. Rep.*, vol. 848, p. 1, 2020.

[5] H. Weng, *et al*., "Large-gap two-dimensional topological insulator in oxygen functionalized MXene," *Phys. Rev. B*, vol. 92, no. 7, p. 075436, 2015.

[6] A. Sarycheva, *et al*., "Two-dimensional titanium carbide (MXene) as surface-enhanced Raman scattering substrate," *J. Phys. Chem. C*, vol. 121, no. 36, p. 19983, 2017.

[7] Y. I. Jhon, Y. M. Jhon, and J. H. Lee, "Broadband ultrafast photonics of two-dimensional transition metal carbides (MXenes)," *Nano Futures*, vol. 4, no. 3, p. 032003, 2020.

[8] Y. I. Jhon, Y. M. Jhon, and J. H. Lee, "Nonlinear optics of MXene in laser technologies," *J. Phys. Mater.*, vol. 3, no. 3, p. 032004, 2020.

[9] Y. I. Jhon, *et al*., "Metallic MXene saturable absorber for femtosecond mode-locked lasers," *Adv. Mater.*, vol. 29, no. 40, p. 1702496, 2017.
[10] K. Y. Lau, X. Liu, and J. Qiu, "MXene saturable absorbers in mode-locked fiber laser," *Laser Photonics Rev.*, vol. 16, no. 9, p. 2100709, 2022.
[11] J. Wang, Z. Xie, G. Lu, J. A. Liu, and J. T. Yeow, "An infrared photothermoelectric detector enabled by MXene and PEDOT: PSS composite for noncontact fingertip tracking," *Microsyst. Nanoeng.*, vol. 9, no. 1, p. 21, 2023.
[12] D. B. Velusamy, *et al*., "MXenes for plasmonic photodetection," *Adv. Mater.*, vol. 31, no. 32, p. 1807658, 2019.
[13] K. Chaudhuri, M. Alhabeb, Z. Wang, V. M. Shalaev, Y. Gogotsi, and A. Boltasseva, "Highly broadband absorber using plasmonic titanium carbide (MXene)," *ACS Photonics*, vol. 5, no. 3, p. 1115, 2018.
[14] D. Zhang, D. Shah, A. Boltasseva, and Y. Gogotsi, "MXenes for photonics," *ACS Photonics*, vol. 9, no. 4, p. 1108, 2022.
[15] K. Hantanasirisakul and Y. Gogotsi, "Electronic and optical properties of 2D transition metal carbides and nitrides (MXenes)," *Adv. Mater.*, vol. 30, no. 52, p. 1804779, 2018.
[16] K. Chaudhuri, *et al*., "Optical properties of MXenes," in *2D Metal Carbides and Nitrides (MXenes): Structure, Properties and Applications*, Cham, Springer, 2019, pp. 327−346.
[17] M. Han, *et al*., "Tailoring electronic and optical properties of MXenes through forming solid solutions," *J. Am. Chem. Soc.*, vol. 142, no. 45, p. 19110, 2020.
[18] M. Jiang, D. Wang, Y. H. Kim, C. Duan, D. V. Talapin, and C. Zhou, "Evolution of surface chemistry in two-dimensional MXenes: from mixed to tunable uniform terminations," *Angew. Chem.*, vol. 63, no. 37, p. e202409480, 2024.
[19] V. Kamysbayev, *et al*., "Covalent surface modifications and superconductivity of two-dimensional metal carbide MXenes," *Science*, vol. 369, no. 6506, p. 979, 2020.
[20] A. A. Shamsabadi, *et al*., "The evolution of MXenes conductivity and optical properties upon heating in air," *Small Methods*, vol. 7, no. 10, p. 2300568, 2023.
[21] L. Liu, *et al*., "Exfoliation and delamination of $Ti_3C_2T_x$ MXene prepared via molten salt etching route," *ACS Nano*, vol. 16, no. 1, p. 111, 2021.
[22] J. Jiang, L. Qin, J. Halim, P. O. A. Persson, L. Hou, and J. Rosen, "Colorless-to-colorful switching of electrochromic MXene by reversible ion insertion," *Nano Res.*, vol. 15, no. 4, p. 3587, 2022.
[23] O. Reshef, I. De Leon, M. Z. Alam, and R. W. Boyd, "Nonlinear optical effects in epsilon-near-zero media," *Nat. Rev. Mater.*, vol. 4, no. 8, p. 535, 2019.
[24] S. Saha, *et al*., "Tailoring the thickness-dependent optical properties of conducting nitrides and oxides for epsilon-near-zero-enhanced photonic applications," *Adv. Mater.*, vol. 35, no. 34, p. 2109546, 2023.
[25] M. Shekhirev, C. E. Shuck, A. Sarycheva, and Y. Gogotsi, "Characterization of MXenes at every step, from their precursors to single flakes and assembled films," *Prog. Mater. Sci.*, vol. 120, p. 100757, 2021.
[26] P. A. Rasheed, R. P. Pandey, F. Banat, and S. W. Hasan, "Recent advances in niobium MXenes: synthesis, properties, and emerging applications," *Matter*, vol. 5, no. 2, p. 546, 2022.
[27] G. A. Niklasson, C. G. Granqvist, and O. Hunderi, "Effective medium models for the optical properties of inhomogeneous materials," *Appl. Opt.*, vol. 20, no. 1, p. 26, 1981.
[28] E. McCann and M. Koshino, "The electronic properties of bilayer graphene," *Rep. Prog. Phys.*, vol. 76, no. 5, p. 056503, 2013.
[29] K. Maleski, C. E. Ren, M. Q. Zhao, B. Anasori, and Y. Gogotsi, "Size-dependent physical and electrochemical properties of two-dimensional MXene flakes," *ACS Appl. Mater. Interfaces*, vol. 10, no. 29, p. 24491, 2018.
[30] M. K. Xu, *et al*., "Electrically conductive $Ti_3C_2T_x$ MXene/polypropylene nanocomposites with an ultralow percolation threshold for efficient electromagnetic interference shielding," *Ind. Eng. Chem. Res.*, vol. 60, no. 11, p. 4342, 2021.
[31] B. Xu, H. Xiang, L. Wei, J. Yin, and Y. Huang, "Band structure engineering of MXenes for low-loss visible epsilon-near-zero properties by first-principles calculation," *Adv. Electron. Mater.*, vol. 9, no. 5, p. 2201119, 2023.
[32] L. J. Prokopeva, S. Peana, and A. V. Kildishev, "Gaussian dispersion analysis in the time domain: efficient conversion with Pade approximant," *Comput. Phys. Commun.*, vol. 279, p. 108413, 2022.
[33] G. Moody, *et al*., "Intrinsic homogeneous linewidth and broadening mechanisms of excitons in monolayer transition metal dichalcogenides," *Nat. Commun.*, vol. 6, no. 1, p. 8315, 2015.
[34] Y. U. Lee, *et al*., "Strong nonlinear optical response in the visible spectral range with epsilon-near-zero organic thin films," *Adv. Opt. Mater.*, vol. 6, no. 14, p. 1701400, 2018.
[35] S. Shrestha, *et al*., "Machine intelligence accelerated design of conductive MXene aerogels with programmable properties," *Nat. Commun.*, vol. 15, no. 1, p. 4685, 2024.
[36] M. Han, *et al*., "Versatility of infrared properties of MXenes," *Mater. Today*, vol. 64, p. 31, 2023.
[37] T. S. Mathis, *et al*., "Modified MAX phase synthesis for environmentally stable and highly conductive Ti_3C_2 MXene," *ACS Nano*, vol. 15, no. 4, p. 6420, 2021.

Supplementary Material: This article contains supplementary material (https://doi.org/10.1515/nanoph-2024-0769).